IEEE Access
Multidisciplinary | Rapid Review | Open Access Journal

Received September 26, 2019, accepted October 8, 2019, date of publication October 11, 2019, date of current version October 23, 2019.

Digital Object Identifier 10.1109/ACCESS.2019.2946736

Review of Active Millimeter Wave Imaging Techniques for Personnel Security Screening

ZHONGMIN WANG[1,2], TIANYING CHANG[1,2], AND HONG-LIANG CUI[2,3]

[1]Institute of Automation, Qilu University of Technology (Shandong Academy of Sciences), Jinan 250014, China
[2]College of Instrumentation and Electrical Engineering, Jilin University, Changchun 130012, China
[3]Chongqing Institute of Green and Intelligent Technology, Chinese Academy of Sciences, Chongqing 400714, China

Corresponding author: Tianying Chang (tchang@jlu.edu.cn)

This work was supported in part by the National Natural Science Foundation of China under Grant 61875196, and in part by the Department of Science and Technology of Shandong Province under Grant 2017GSF20114.

ABSTRACT This paper reviews recent progress of active millimeter wave (mmW) imaging techniques for personnel security screening. With the ability to penetrate clothing and the promised millimeter scale spatial resolution, mmW imaging has been widely pursued for personnel surveillance without the usual concern for radiation safety. A brief development history of mmW imaging is introduced. An overview of imaging research and developmental achievements, along with antenna considerations based on quasi-optical geometry, phased reflector array, monostatic array, and multistatic array, is provided. Design considerations related to practical applications, including system calibrations, walk-through system (WTS), portable system, and compressive sensing (CS), are also discussed.

INDEX TERMS Millimeter wave imaging, personnel security screening, review.

I. INTRODUCTION

Millimeter wave (mmW) imaging is now widely used for personnel security screening at airports, security check points and other relevant public or military areas [1], [2]. MmW is electromagnetic wave usually defined to be within nominal wavelength of 1∼10 mm (30∼300 GHz). Based on a half power criterion, most clothing is transparent for mmW [3], and imaging systems using mmW are capable of penetrating common clothing barriers to form an image of a person as well as any concealed objects. Since diffraction generally limits resolution to spot sizes of about half wavelength, millimeter scale spatial resolution is readily achievable [4]. Additionally, mmW is nonionizing, and needs 10,000 times less power than cell phones to illuminate a person under surveillance [5]. By virtue of these unique advantages, mmW imaging techniques could achieve detection of concealed threats of metallic and nonmetallic objects, e.g., plastic and liquid explosives, ceramic knives, contrabands, and narcotics [2], [6]. The current state of the art for mmW imaging systems comprises several technologies including active and passive mmW imaging. Active mmW imaging systems have several advantages over passive systems including elimination of bulky lenses or reflectors, high signal to noise ratio (SNR) operation, high contrast for detection of concealed objects [7], and as such has become the mainstream technology. By 2018, more than 2,000 active mmW imaging systems for personnel security screening had been deployed at airports in the United States, Britain, the Netherlands, Australia, Japan, and China [8]. The United States, European Union and China all have promulgated technical standards for mmW personnel security screening systems [9].

Active mmW imaging uses artificially generated radiation to illuminate the scene, and the reconstructed image is achieved by the scene's reflectance distribution [10]. Obtaining an image of a scene could be carried out in many different imaging system structures, such as scanned single element, focal plane array, phased array and synthetic aperture radar (SAR) [11].

The scanned single element imaging structure is achieved either by moving a receiver in the focal plane of an antenna or scanning the beam direction. In 1971, Farhat and Guard used 70 GHz mmW in working toward imaging of concealed weapons [12]. The phase distribution of scattered field by an ordinary metallic toy gun is determined by mechanically scanning a harmonic mixer over a 0.75 m diameter circular aperture in a spiral pattern, and the reconstructed image is achieved by optical holography reconstruction

The associate editor coordinating the review of this manuscript and approving it for publication was Davide Comite.

technique. In 2008, Cooper et al. applied the scanning of a single element transceiver with frequency modulated continuous wave (FMCW) technique to the detection of concealed objects on a person, and the presented a system operating at 576∼605 GHz that can image a torso with 1 cm resolution at 4 m standoff distance in about five minutes [13], [14]. In 2009, Sheen et al. used a quasi-optical focusing system and high-speed conical scanner to develop a standoff three-dimensional (3D) imaging prototype operating near 350 GHz [4], [15]. The system allows screening at ranges of 2∼10 m, and obtains an image in 10 s. In 2012, Robertson et al. used a pair of galvanometer mounted mirrors to scan a mmW beam rapidly in azimuth and elevation over a limited field of view (FOV), and achieved 340 GHz imaging radar operation with 10 Hz frame rate [16]. The existing scanned single element imaging radar readily achieves large standoff distance detection, has moderate size with compact optics, allows a free flow of personnel as they were being screened, but suffers from the relatively unreliable mechanical scanning systems together with low data transfer rate.

The focal plane array imaging radar employs an array of independent receivers in the focal surface of an imaging large lens. In 1991, Goldsmith et al. used a 64-element focal plane array employing slot antennas to develop an active mmW quasi-optical concealed object detection system. The imaging optics consisting of a pair of plano-convex lenses with curved surfaces facing together is designed to maximize the FOV over which a uniform focused spot size could be obtained. The imaging distance is about 90 cm, and the waist radius at the focused spot is 0.55 cm [11], [17]. In 2013, Andrews et al. presented a mmW radar using a Gaussian optic lens antenna for concealed threats detection. The radar system is portable and manually steered by the operator to enable up to 25 m standoff distance for monitoring walking human targets at video frame rates [18]. Imaging radar using multiple receiver arrays in the focal plane of the imaging optics has possible real time operation and relative compactness. However, the resolution is relatively low due to the high optical F-number of a practical optics configuration, and the FOV is usually limited by the small aperture size.

The phased array imaging system synthesizes beams from a number of independent radiating elements. The representative commercial system is the Eqo people screening system developed by Smiths Detection Inc. The system employs a phased reflector array applying the binary phase approximation to steer and focus the mmW to a specific point in the FOV [15], [19]. The mmW beams are sensitive to radiation arriving from different directions by use of the phased array, while it is difficulty to design efficient radiating elements, and the binary phase approximation as a compromise method is used in the system.

SAR has been the most popular technique used in active portal mmW imaging systems. In SAR, an antenna array instead of a quasi-optical aperture achieves large-aperture operation, and the phase and amplitude of the scattered signal are recorded without the need for optical lens. In the 1990s, Collins et al. dramatically improved the original quasi-optical aperture mmW imaging technique by utilizing a scanned transceiver and digital focusing technique [20]–[22]. In 2001, Sheen et al. developed a near-field planar wideband holographic mmW imaging system. A prototype imaging system utilizing a 27∼33 GHz linear sequentially switched array and a high-speed linear scanner was developed and tested [5]. In 2006, Sheen et al. developed a wideband mmW cylindrical imaging system, which was commercialized by L3 Security and Detection Systems, Inc., and improved by using higher frequency ranges up to 100 GHz and polarimetric imaging techniques [23]–[25]. A vertically oriented linear array that sweeps out a cylindrical aperture using a mechanical scanner is used. A full 360° volumetric reconstruction is achieved by gathering data over a full 360° cylindrical aperture [26]. The system throughput is about 300∼600 people per hour depending on the application. Compared to planar techniques, cylindrical imaging could inspect the person from all angles with a single scanning.

The planar and cylindrical imaging techniques are both based on monostatic or quasi-monostatic arrays, requiring that a transceiver be physically scanned over a two-dimensional (2D) aperture, which could result in high order artifacts and a slow process [27]. To mitigate the appearance of high order artifacts in images due to multipath effects of the monostatic measurement configuration, Fernandes et al. developed a multistatic array configuration with a generalized SAR in 2011 [28]. However, it does not lend itself to Fourier-based fast reconstruction algorithms, and requires vast parallel computing. In 2011, Ahmed developed a fully electronic active mmW imaging system based on a planar multistatic sparse array. The 72∼80 GHz mmW imaging system achieves images with cross-range resolution of 2 mm, 30 dB dynamic range, and measurement time of a few hundred milliseconds [29].

In recent years, some improvements based on the classical quasi-optical or digital focusing techniques have been made for enhancing the mmW imaging systems' practicability. To suppress speckles and reduce system complexity and cost, several non-imaging techniques were proposed. In 2011, Radenamad et al. proposed amplitude modulation (AM) mmW imaging system using the envelope phase detection method [30]. The proposed method could suppress harmful speckles, and render the shape of the object more clearly. In 2013, Andrews et al. designed a linearly polarized 75∼110 GHz 25 m standoff mmW system with a Gaussian optic lens antenna, with the receivers only measured the power of the signals scattered by the target [18]. The system was portable and detected on-the-move human targets at 30 fps video frame rates. In 2014, Onojima et al. proposed an mmW imaging system using a complex-valued self-organizing map (CSOM), and realized adaptive clustering of complex-valued texture in space and frequency domain to reconstruct image. The system was especially suitable for detecting object having mirror glaring and speckles [10].

To improve the throughput, the concept of a mmW walk-through system (WTS) was proposed in 2016 by Gumbmann and Ahmed, based on the perimeter multistatic sparse array [31]. In the same year, Gonzalez-Valdes et al. designed a WTS based on inhomogeneous multistatic sparse array [32]. Multiple frame images could be achieved during the movement of the passenger while passing through the WTS, and the detection performance could be enhanced since possible concealed threats are visible from different perspectives and could be tracked within different frames.

To resolve the conflict between compactness requirements in applications and mannequin FOV as well as reasonable cross-range resolution, the portable imaging systems combing mmW imaging and optical camera or positioning system are proposed after 2017 [33], [34]. With the spatial information provided by the optical auxiliary systems, the compact aperture is equivalently synthesized to produce a large effective aperture, and the multiple frames are fused together for reconstructing the image.

Additionally, the compressive sensing (CS) signal processing technique was also used in mmW imaging systems for reducing the number of antennas, as well as system cost and complexity. From 2015 to 2017, several mmW imaging systems using CS based on monostatic array [35], bistatic array [36], cylindrical configuration [37] and planar phased array [38], [39] were proposed. The related experiments showed that CS had the advantages of reducing the scanning time and improving the reconstructed image quality.

In addition to the brief overview of the development highlights of mmW active imaging techniques for personnel screening to date, this paper gives a comprehensive review of research activities and technical achievements in this area, including antenna array design considerations for active mmW imaging systems. We hope that this paper will provide valuable information to readers interested in research and application of mmW imaging systems.

This paper is organized as follows. Section II introduces electromagnetic theory fundamental for mmW imaging. Section III reviews the imaging techniques for mmW imaging systems based on quasi-optical focusing, SAR based digital focusing and non-imaging method. Considerations in practical applications for personnel security screening, including system calibrations, WTS and CS, are discussed in Section IV. Finally, Section V concludes the paper with a brief summary and outlook.

II. THEORETICAL FUNDAMENTALS

MmW imaging techniques achieve reflectivity distribution of the imaged object using scattered signal, and are essentially based on the solution of the electromagnetic inverse scattering problem. Scattered signal is studied starting from the wave equation [40], whose solution is briefly discussed here, with detailed derivation from the Maxwell's equations given in the Appendix.

When electromagnetic wave travels in a uniform non-magnetic medium, the homogeneous Helmholtz equation is obtained (see Eq. A4 of the Appendix)

$$\nabla^2 \boldsymbol{E} + k_0^2 \varepsilon_r^c(r)\, \boldsymbol{E} = 0, \tag{1}$$

where k_0 is the wavenumber in free space, and $\varepsilon_r^c(r)$ the complex relative permittivity.

The vector field $\boldsymbol{E}$ is replaced by the scalar field U that represents a component of the vector field, which satisfies an inhomogeneous Helmholtz equation of the form

$$\nabla^2 U^s + k_0^2 U^s = -O(r) \cdot U, \tag{2}$$

where $U = U^i + U^s$, U^i and U^s represent the incident and scattered scalar field, $O(r) = k_0^2(\varepsilon_r^c(r) - 1)$ is an effective scattering potential introduced by Wolf, containing the imaged object information [41].

Based on the first-order Born approximation and Green's function describing an outward propagating spherical wave emanating from the transmitter, (2) becomes

$$U^s(r) = \iiint O\left(r'\right) \cdot U\left(r'\right) G(r - r')dr', \tag{3}$$

where $G\left(r - r'\right) = \frac{e^{-jk_0(r-r')}}{4\pi(r-r')}$ is the Green's function, r' an arbitrary vector in the source domain.

In an active mmW personnel security screening system, the observed image is dependent on the electromagnetic properties of clothing, skin and contrabands, which are functions of their scattering potential i.e. the reflective properties of the materials [42]. Reflectivity and transmission measurements of several common materials at 100 GHz are shown in Table 1 [11]. Clothing have reflectivity in the range of -30 to -13 dB, while the reflectivity of various portions of the human body ranges from -15.0 to -8.4 dB. Dielectric contraband materials such as ceramic, polycarbonate and polypropylene have reflectivity in the range of -8.8 to -4.5 dB, and metallic contrabands have total reflection characteristic. It is clearly that contraband materials have reflectivity 2$\sim$4 times that of human skin, and clothing provides negligible reflectivity. Since higher reflectivity of the imaged object results in a higher brightness in the reconstructed image, contrabands could be identified.

TABLE 1. 100-GHz measurements of clothing, skin, and contrabands.

Sample		Thickness (mm)	Reflection (dB)	Transmission (dB)
Clothing	Wool	1.4	-13	-0.8
	Nylon	0.1	-23	-0.1
	Flannel	0.5	-18	-0.3
	Denim	1.0	-30	-0.3
	Leather	0.8	-18	-0.7
	Corduroy	0.6	-16	-0.4
Skin	Calf	Null	-11.3	Null
	Forearm	Null	-8.4	Null
	Jowl	Null	-15.0	Null
	Chest	Null	-8.8	Null
Contrabands	Ceramic	2.6	-4.5	-3.0
	Polycarbonate	5.5	-8.5	-1.8
	Polypropylene	1.5	-8.8	-0.8
	Metal	Null	0	Null

III. IMAGING TECHNIQUES

Since the basic premise of electromagnetic wave imaging is to utilize the known measurements of scattering and incidence field distributions to achieve the characteristic distributions of scattering parameters in the imaging area, the scattered field $U^s(r)$ can be focused by an imaging system that will reveal the size, shape, and orientation of the imaged object. Intuitively, the image related term $O\left(r'\right)$ could be obtained by solving the partial differential equation about the $U^s(r)$. For electromagnetic wave in the Rayleigh region, the common method for solving the inverse scattering problem is to utilize the static field analysis to achieve the electrical parameter distributions in space. Unfortunately, the analytical method is very complex and time-consuming, and not usually adopted in practical imaging systems. Thanks to the great Joseph Fourier for opening the door to frequency domain, the inverse scattering problem i.e. focusing for imaging could be solved conveniently by Fourier transform (FT) between space-time and wavevector-frequency domain. The Fourier transform operations can be performed either optically by a convergent lens or digitally by a processor usually employing fast Fourier transform (FFT) algorithms [43]–[45].

The preferred focusing technique is different for specific applications. Mmw imaging systems could be operated in portal or standoff configuration, and the detection range of the later could be up to tens of meters. For standoff range personnel security screening imaging systems, higher frequency electromagnetic wave, even up to submillimeter wavelength, must be used to achieve a spot size of several centimeters in the imaging area. In the several hundred GHz frequency range, heterodyne transceiver array technology and commercial integrated MMIC chips are still in their infancy. Therefore, quasi-optical lens with a single beam relying on mechanical scanning are preferred. In contrast, SAR with digital focusing is used in portal approaches. In near distance personnel security screening systems, mmW below 100 GHz is usually used. And related commercial transceivers, as well as auxiliary RF devices, have developed into maturity along with the development of the automotive mmW radar and the 5th generation wireless systems. Therefore, the emission and reception of mmW are achieved by antennas arrays with mechanical or electrical scanning, and focusing is performed digitally in a backend processor.

A. QUASI-OPTICAL FOCUSING

Early in 1971, the original mmW imaging system for concealed weapons used two lenses for image reconstruction behind the mmW illumination part [12]. A reflex klystron phase-locked to the local oscillator (LO) of a coherent receiver produced 70 GHz continuous wave (CW). A parabolic antenna emitted mmW to the imaging area, and a pyramidal horn with spiral scanning detected the scattering wave from the targets. A harmonic mixer mixed the echo signal and the LO signal, and sent the intermediate frequency (IF) signal to the receiver. The simplified block

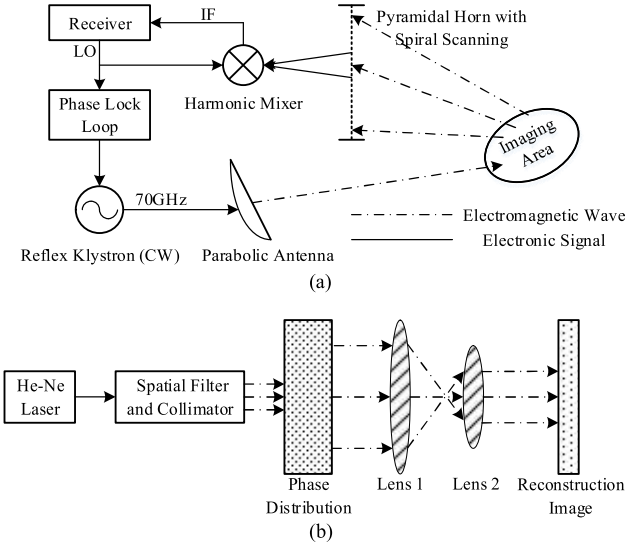

FIGURE 1. Block diagram of illumination (a) and image reconstruction (b) in the original mmW imaging system.

diagram of mmW illumination part is shown in Fig. 1 (a). The phase distribution of the imaged object is illuminated with a spatially filtered and collimated He-Ne laser beam, and reconstructed the real image of the object by use of two lenses. The image reconstruction arrangement is shown in Fig. 1 (b). The reconstructed image of a toy metal gun, which was placed 1.25 m distance in front of the aperture and under the clothes, was achieved by use of the system.

Apparently, the quasi-optical focusing system could be also combined with the illumination system. There are several comparatively mature active submillimeter wave imaging systems for personnel security screening developed by SynView, Pacific Northwest National Laboratory (PNNL), and NASA Jet Propulsion Laboratory (JPL). In the active 645 GHz system developed by SynView [46], the quasi-optical system consists of two lenses, three mirrors and a beam splitter, as shown in Fig. 2 (a). The collimator lens collimates the beam emitted by the source. The beam is then divided into two parts by the beam splitter, one part is absorbed while the other passes the beam splitter. The spherical mirror with 102 mm diameter conducts the beam to the primary elliptical mirror with 230 mm diameter, and the large plane scanning mirror with 320 mm diameter concentrates the beam onto one object point. The reflected beam from the beam splitter is focused onto the detector by the focusing lens. The plane scanning mirror has 5 ° angle of inclination with respect to its fast spinning axis, and an elliptical scan trail is achieved. The plane mirror is also rotated slowly about the vertical axis perpendicular to the fast one, and horizontal shift of the elliptical trail is realized. The resulting FOV looks like a cycloid region. Additionally, SynView also developed a similar system with 300 GHz.

In the active 350 GHz mmW standoff imaging system presented by PNNL [4], [15], the quasi-optical focusing system consists of a focusing reflector and a circular plane mirror,

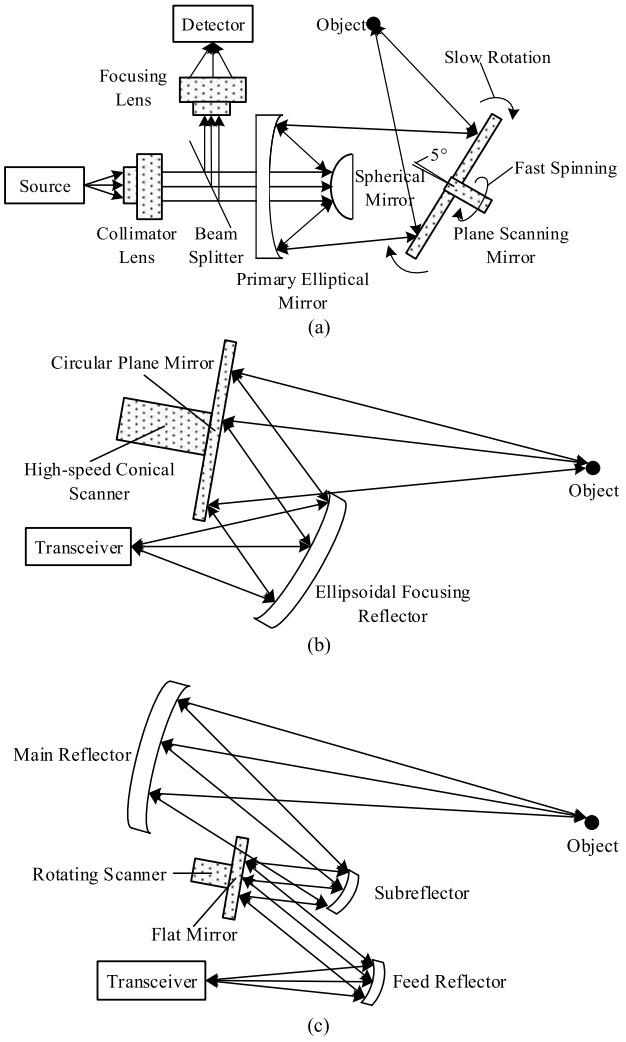

FIGURE 2. Active submillimeter standoff quasi-optical focusing systems developed by SynView (a), PNNL (b), and JPL (c).

as shown in Fig. 2 (b). The focusing reflector with 500 mm diameter is illuminated by the beam from the transceiver, and the circular plane mirror concentrates the beam to an object point. The conical scanner steers the circular plane mirror, which is mounted with a slight wedge. The wedge offsets the deviation angle, and the object point traces out a circular pattern when the mirror is rotated. The circular pattern is then scanned vertically to fill out the imaging area, and the FOV is an oval region.

The two systems described above have a lot in common. Both of them have a fully electronic FMCW heterodyne transceiver coupled to a quasi-optical focusing system, utilize a circular plane mirror with rotating and tilt scanning to form the 2D FOV. The quasi-optical focusing design could minimize aberrations and allow for significantly off-axis performance with minimal degradation.

Compared to the systems presented by SynView and PNNL, the 675 GHz imaging system developed by JPL has several improvements for increasing the imaging speed as well as the standoff distance. Both of the SynView's and PNNL's systems rely on steering the beam after the main ellipsoidal focusing reflector, making them difficult to be used with large diameter apertures, resulting in limited working distance with reasonable resolution. In the JPL's system, the beam scanning is achieved by the lightweight flat mirror placed in the feed optics of the main reflector with only 130 mm diameter deflected over about ±2.5° in elevation and azimuth, and the corresponding beam covering is ±20 cm in the horizontal and vertical directions at 25 m standoff distance, as shown in Fig. 2 (c) [47]–[51]. The idea of using a small lightweight flat mirror is beneficial to reduce the scanning time and increase the imaging speed. The scanning flat mirror is illuminated by a collimated beam rather than an expanding beam, and the design relaxes the tolerances on the position of the scanning mirror's principal axes, which otherwise would be difficult to align at 675 GHz. Without rotating operation, the bigger main reflector could be used to get farther standoff distance. Beside fast scanning, the angular position of the flat mirror is controlled precisely by use of a servomotor and a rotary encoder, and aberrations are suppressed dramatically. Furthermore, a bifocal ellipsoidal Gregorian reflector system (BEGRS) based on the confocal Gregorian subsystem used in JPL's system is designed by García-Pino *et al.* [52]. The nominal reflector surfaces are substituted by shaped surfaces to reduce the beam aberrations, and the FOV of the imaging system could be increased. Based on the quasi-optical focusing system in Fig. 2 (c), the FOV-enhanced 300 GHz imaging system, in which the main reflector and the subreflector are shaped surfaces designed as a BEGRS, was proposed by Grajal *et al.* [53], [54]. The specifications of the four active standoff imaging systems are listed in Table 2.

Additionally, a phased reflector array applying binary phase approximation to focus mmW to an object point is utilized in the commercial Smith Detection eqo^{TM} system [19], (the technology is licensed from Agilent Technologies [55]), as shown in Fig. 3. The transceiver emits 25 GHz mmW

TABLE 2. Specifications of active standoff imaging systems developed by SynView, PNNL, JPL, and Grajal *et al.*

Specifications	SynView	PNNL	JPL	Grajal et al.
Center frequency	645 GHz	350 GHz	675 GHz	300 GHz
Bandwidth	10 GHz	9.6 GHz	28.8 GHz	27 GHz
Primary aperture diameter	23 cm	50 cm	100 cm	60 cm
Imaging speed	9 s (Measurement time)	10 s	1 s	0.5 s
Standoff distance	0.75~1.5 m	2~10 m	4~25 m	8 m
FOV	20 cm by 30 cm at 1 m	1.25 m by 2.5 m at 5 m	0.4 m by 0.4 m at 25 m	0.5 m by 0.9 m at 8 m
Lateral resolution	4 mm at 1 m	10 mm at 5 m	5 mm at 4 m	16 mm at 8 m
Range resolution	42 cm	Null	0.7 cm	1 cm

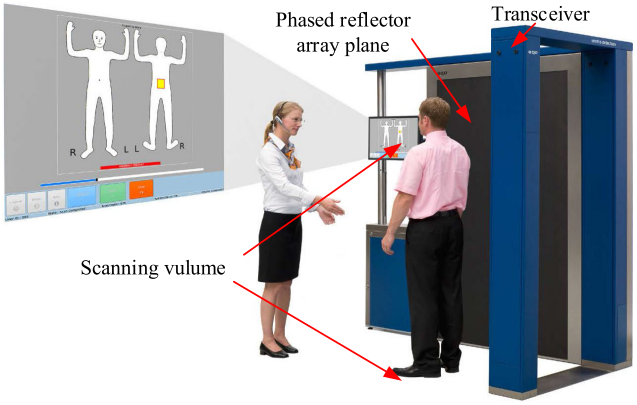

FIGURE 3. Smith Detection eqo™ system.

directionally toward the phased reflector array plane, and the beam is then reflected, steered, and focused on a specific point in the scanning volume by programming the phased reflector array. According to the reciprocity principle, the reflected wave from the specific point is redirected back to the transceiver. The reconstructed image is achieved by use of amplitude, phase and location information of each point in the scanning volume [56], [57]. The scanning volume is 1.1 m wide by 2 m high by 1 m standoff distance, and a subject rotating with raised hands within the FOV is needed.

B. DIGITAL FOCUSING IN MONOSTATIC ARRAY

Currently, the more mature active mmW imaging systems use SAR to achieve large aperture and digital focusing to reconstruct image for portal personnel security screening. More specifically, the monostatic array is the most common configuration because of simple structure and low cost in the existing mmW imaging systems [5], [35], [58], [59], [60]. Generally, a linear antenna array is electronically scanned over an axis, e.g., horizontal axis, while the linear array is mechanically wept over another axis, e.g., vertical axis. The antenna array includes two rows or columns containing transmitting and receiving antennas respectively, and the interval between them is small enough to assume that the transceiver antenna pair to have the same location. At the same time, only a pair of co-located transceiver antennas transmit and receive mmW. And the 2D planar aperture is achieved by use of mechanical or electrical scanning [61], [62]. The photographs of several monostatic antenna array examples in existing mmW imaging system are shown in Fig. 4, and the photographs of the commercial ProVision2 active portal system based on monostatic array and cylindrical scanning developed by PNNL is shown in Fig. 5.

To facilitate the description of digital focusing in a monostatic array, the notations used in SAR imaging (ignoring the constant factor under the integral sign) are adopted. Then, (3) is rewritten as

$$s(x_0, y_0, z_0, k) = \iiint \frac{1}{R_1 R_2} f(x, y, z)\, e^{-jk(R_1+R_2)} dxdydz, \tag{4}$$

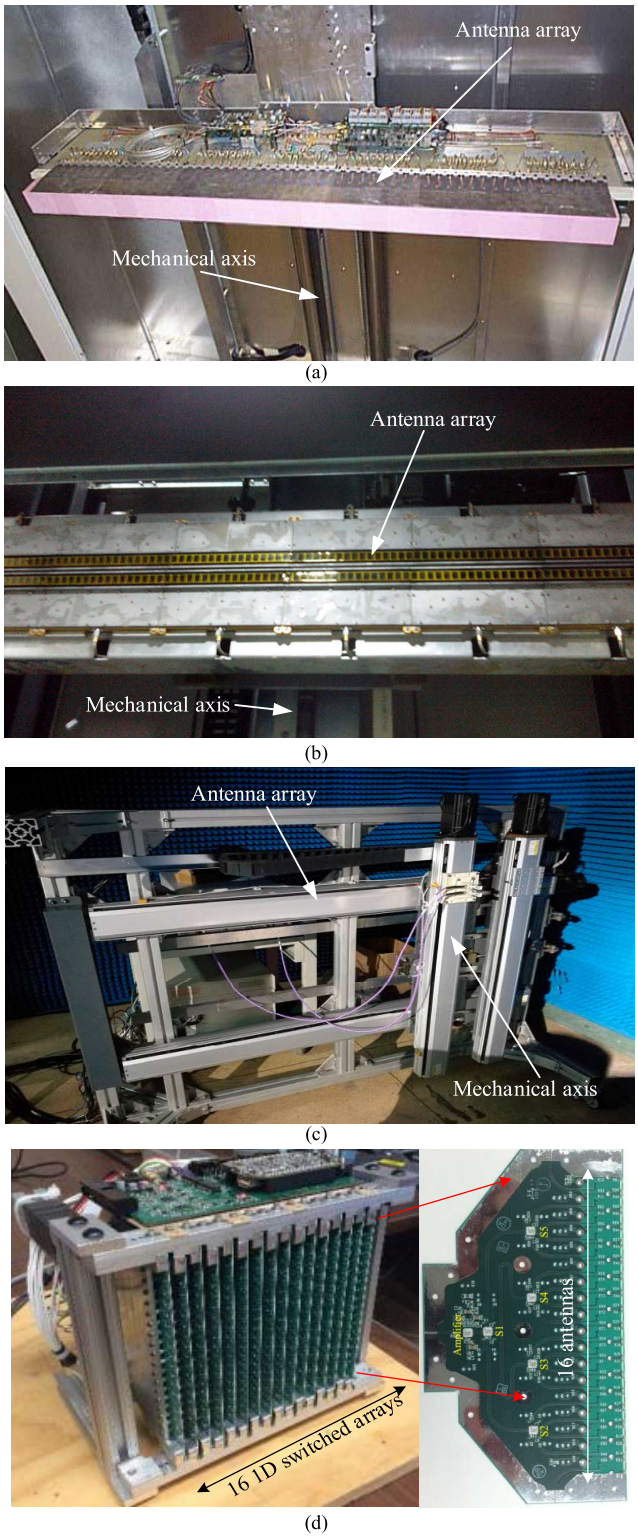

FIGURE 4. Optical images of the monostatic antenna arrays developed by PNNL (a), Nuctech (b), Ye Zhang (c) and M. T. Ghasr (d).

where $s(x_0, y_0, z_0, k)$ denotes the scattering signal at the Cartesian coordinate (x_0, y_0, z_0), z_0 is usually supposed to be zero and ignored, k the mmW wavenumber, R_1 and R_2 the propagation distance associated with transceiver and imaged object location, $f(x, y, z)$ the imaged object reflectance at

FIGURE 5. Optical images of commercial ProVision2 mmW imaging system.

(x, y, z) within the imaging region. Of course, the concrete forms about $s(x_0, y_0, z_0, k)$, R_1 and R_2 vary with antenna configuration in a specific imaging system.

Since the transmitter and receiver have the same location for a monostatic array, (4) becomes

$$s(x_0, y_0, k) = \iiint \frac{1}{R^2} f(x, y, z)\, e^{-j2kR} dxdydz, \quad (5)$$

where $R = \sqrt{(x - x_0)^2 + (y - y_0)^2 + z^2}$ represents the round trip distance between the transceiver and the imaged object. It must be noted that the propagation loss factor $\frac{1}{R^2}$ is commonly omitted.

The mmW digital focusing technique originates from the optic holography technique, which relies on measurement of the wavefront magnitude and phase scattered from the imaged object and was first proposed by D. Gabor in 1948 [63]. The original mmW digital focusing algorithm is called holographic image reconstruction algorithm by Sheen *et al.* [22]. Actually, the optic holography technique aroused great interest amongst radar researchers and directly resulted in the birth of SAR in the 1960s. The range migration algorithm (RMA) used in SAR was first proposed by Soumekh in 1991 [64], [65]. Although SAR differs significantly from the quasi-optic holography technique, e.g., SAR generally uses rectilinear aperture and mostly pertains to side-looking radar, while the quasi-optic holography has planar aperture and front view radar [27], [66]. However, the differences do not affect scattering signal processing steps. Both of them have four key steps, the Fourier transform, the phase linearity, the interpolation in frequency domain, and the inverse Fourier transform, and all of them are core steps in RMA.

By applying 2D Fourier transform, (5) becomes

$$S(k_x, k_y, k) = \iiint \iint f(x, y, z)\, e^{-j2kR} e^{-jk_x x_0} e^{-jk_y y_0} dx_0 dy_0, dxdydz \quad (6)$$

where $S(k_x, k_y, k)$ represents the 2D Fourier transform of $s(x_0, y_0, k)$, k_x and k_y the wavenumber in the x and y directions, respectively.

The double integral term in (6) could be rewritten in phase linearity form by applying the Method of Stationary Phase (MSP), or the equivalent approximation method that a spherical wave is decomposed into a superposition of plane wave components [5]. And (6) could be rewritten to

$$S(k_x, k_y, k) = \iiint f(x, y, z)\, e^{-jk_x x} e^{-jk_y y} e^{-jk_z z} dxdydz, \quad (7)$$

where $k_z = \sqrt{(2k)^2 - k_x^2 - k_y^2}$ denotes the wavenumber in the z direction.

Since $S(k_x, k_y, k)$ is nonuniformly spaced in k_z, an additional Stolt interpolation step is usually used to realize uniform resample in k_z. By applying 3D inverse Fourier transform, the imaged object reflectance $f(x, y, z)$ can be obtained as

$$f(x, y, z) = FT_{3D}^{-1}\left(Stolt\left(FT_{2D}\left(s(x_0, y_0, k)\right)\right)\right), \quad (8)$$

where $FT_{3D}^{-1}()$ means the 3D inverse Fourier transform, $FT_{2D}()$ the 2D Fourier transform.

RMA is rendered tractable by several important approximations, such as Stolt interpolation, omission of propagation loss and multiple reflections. The approximation during the Stolt interpolation processing induces inevitable errors. To overcome this deficiency, nonuniform Fourier transform or coherence factor could be used in RMA [67], [68]. To compensate mmW propagation loss and improve reconstructed image quality in the range direction, the data after inverse Fourier transform could be compensated by factors derived from scalar diffraction theory [69]–[71].

In order to inspect a person from all angles and reduce the undesirable effects of specular reflection, a cylindrical mmW imaging system is proposed by PNNL [27]. Compared to RMA used in planar systems, the digital focusing algorithm used in wideband cylindrical imaging system requires several additional steps. First, individual arc segments, which are typically 90 ° in width, are reconstructed by RMA. Second, each reconstructed 3D image is collapsed into a 2D image by the maximum value projection. Finally, arc segments are reconstructed at any angle, and the imaged object could be viewed from any aspect angle. Alternatively, eight overlapping 90 degrees 3D images are added to form a single 3D image [27], [72].

In the mmW imaging systems based on monostatic array, the lateral resolution obtained in the reconstructed image is determined by examining the width of the coverage in frequency domain and is limited by diffraction, while the range resolution is determined by mmW bandwidth [5], [27]:

$$\delta_c \approx \frac{\lambda_c R_c}{2D}, \quad \delta_r \approx \frac{C}{2B}, \quad (9)$$

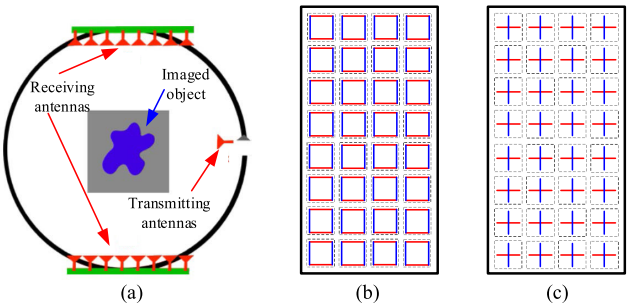

FIGURE 6. (a) Cylindrical multistatic array, (b) perimeter multistatic array, and (c) cross multistatic array.

where δ_c and δ_r represent lateral and range resolution, λ_c is the mmW center frequency, R_c the distance from the antenna plane to the imaged object, D the width of the aperture, C the speed of light, and B the mmW bandwidth.

C. DIGITAL FOCUSING IN MULTISTATIC ARRAY

In practical applications, the imaging speed is a very important technical index for mmW imaging system. However, in monostatic mmW systems, mechanical scan usually limits the improvement of imaging velocity. And it is very costly and impractical to make a fully monostatic electronic solution. Multistatic sparse array mmW imaging systems are then proposed, and three existing multistatic structural configurations are shown in Fig. 6. The blue and red lines in Fig. 6. (b) and (c) represent the linear transmitting and receiving antennas with certain intervals, respectively. The photograph of the commercial QPS100 active portal system based on multistatic arrays and fully electrical scanning developed by Rohde & Schwarz is shown in Fig. 7.

The digital focusing algorithm used in cylindrical multistatic system is based on back propagation algorithm that requires vast parallel computing [28]. The multistatic digital focusing algorithm based on frequency domain, which is actually multi-input-multi-output RMA (MIMO RMA), is used in perimeter multistatic system [29], [73] and is summarized here.

Without loss of generality, a dense MIMO array is used for analysis, whose transmitting and receiving antennas are co-located in a 2D planar region. The scattering signal is

$$s\left(x_T, x_R, y_T, y_R, k\right) = \iiint \frac{1}{R_T R_R} f\left(x, y, z\right) e^{-jk(R_T+R_R)} dxdydz, \quad (10)$$

where (x_T, y_T) and (x_R, y_R) represent the transmitting and receiving antenna location, $R_T = \sqrt{(x_T-x)^2+(y_T-y)^2+z^2}$ and $R_R = \sqrt{(x_R-x)^2+(y_R-y)^2+z^2}$ the distance from the transmitting and receiving antenna to the imaged object, respectively.

Obviously, the scattering signal is a set of 5D data, and must be reduced to 3D spatial data by some dimension reduction method for imaging. The dimension reduction can be realized with one of two approaches, space domain or frequency domain dimension reduction. The former is used in effective phase center principle, and each transmit-receive antenna pair forms an effective phase center, which lies at the midpoint of the two antennas [74], [75]. RMA could be used to reconstructed image then.

FIGURE 7. Optical image of commercial QPS100 mmW imaging system.

Alternatively, the scattering signal is applied a 2D Fourier transform for respective space distribution of transmitter and receiver, and (10) becomes

$$\begin{aligned} &S\left(k_{xt}, k_{xr}, k_{yt}, k_{yr}, k\right) \\ &= \iiint f\left(x, y, z\right) \iint \frac{1}{R_T} e^{-jkR_T} e^{-jk_{xt}x_T} e^{-jk_{yt}y_T} dx_T dy_T \\ &\quad \times \iint \frac{1}{R_R} e^{-jkR_R} e^{-jk_{xr}x_R} e^{-jk_{yr}y_R} dx_R dy_R dxdydz. \end{aligned} \quad (11)$$

By applying MSP to the two double integral terms, we get

$$\begin{aligned} &S\left(k_{xt}, k_{xr}, k_{yt}, k_{yr}, k\right) \\ &= \iiint \frac{f\left(x, y, z\right)}{k_{zt}k_{zr}} e^{-jk_{xt}x-jk_{yt}y-jk_{zt}z} e^{-jk_{xr}x-jk_{yr}y-jk_{zr}z} dxdydz, \end{aligned} \quad (12)$$

where $k_{zt} = \sqrt{k^2 - k_{xt}^2 - k_{yt}^2}$ and $k_{zr} = \sqrt{k^2 - k_{xr}^2 - k_{yr}^2}$.

By applying following identities to realize frequency domain dimension reduction [73]

$$\begin{aligned} k_x &= k_{xt} + k_{xr}, \\ k_y &= k_{yt} + k_{yr}, \\ k_z &= k_{zt} + k_{zr}, \end{aligned} \quad (13)$$

(12) becomes

$$S'(k_x, k_y, k) = \iiint \frac{f(x, y, z)}{k_{zt} k_{zr}} e^{-jk_x x - jk_y y - jk_z z} dxdydz. \quad (14)$$

Similar to RMA, Stolt interpolation and 3D inverse Fourier transform are used at last, and the imaged object reflectance $f(x, y, z)$ can be obtained as

$$f(x, y, z) = FT_{3D}^{-1}\left(Stolt\left(S'(k_x, k_y, k)\right)\right). \quad (15)$$

Not only perimeter or cross multistatic arrays, but also other uniform multistatic arrays with sparsity in general in mmW imaging systems could readily use the modified MIMO RMA to reconstruct the image of an object.

In a mmW imaging system based on multistatic arrays, the lateral and range resolution are given by [29]

$$\delta_{mc} \approx \frac{\lambda_c R_c}{D_t + D_r}, \qquad \delta_{mr} \approx \frac{C}{2B}, \quad (16)$$

where D_t and D_r represent the width of the transmitter and receiver aperture, respectively.

Assuming that D_t, D_r in multistatic array and D in monostatic array all have the same value, the same lateral and range resolution could be obtained. However, the spacing between the antennas for satisfying the Nyquist criterion in a multistatic array is only half of the spacing between the antennas in a monostatic array [75].

Additionally, metasurfaces, a current research focus, have been used in multistatic mmW imaging system with a novel digital focusing technique. To reduce system complexity and cost, a low-profile mmW imaging system using computational imaging with a frequency-diverse metasurface aperture was demonstrated by Gollub *et al.* [76]. In the proposed system, the planar array is composed of 24 transmit and 72 receive metasurface panels, which are distributed over a 2.1 m by 2.1 m aperture, as shown in Fig. 8. The metasurface panel, which is constructed of low-loss copper clad printed circuit substrate, generates distinct complex radiation patterns as a function of frequency. As with the multistatic array configuration, a single transmit panel is repeatedly excited by a 17.5∼26.5 GHz frequency sweep, with measurements taken sequentially on all of the receive panels. With the help of the metasurface panel, the mmW is controlled flexibly, and a diverse set of radiation patterns is achieved for applying the computational imaging approach for solving the electromagnetic inverse scattering problem. Instead of the classical digital focusing technique, the iterative least squares reweighting is used to seek to minimize the objective function $\|g - Hf_{est}\|^2$, where g denotes the measurements, H the measurement matrix and f_{est} the estimation of reflectivity. However, the computational imaging supports a reduction in the complexity of the physical aperture at the expense of increasing the burden of numerical and algorithmic processing.

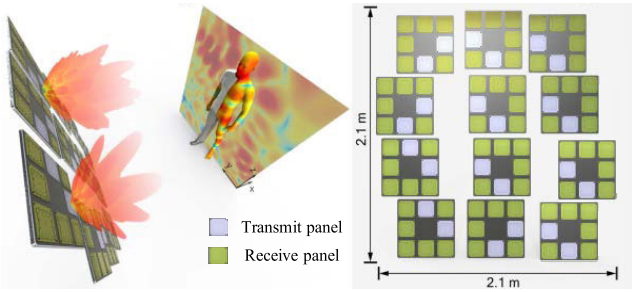

FIGURE 8. Frequency-diverse metasurface planar array.

D. NON-IMAGING TECHNIQUES

Active mmW imaging uses artificially generated electromagnetic wave to illuminate the FOV, and the formed image is dominated by the object's reflectance distribution, which is sensitive to the orientation of reflecting surfaces and their diffusivity and specular reflections [77], [78]. Compared to object with rough surface, flat surface object has higher brightness, known as "speckles" or "glints", which is a harmful effect observed especially in coherent imaging and obstructs object identification. For another, existing active mmW prototypes are unique and expensive. The systems are complicated and need accurate mechanical or electrical scanning in one or two dimensions. To overcome speckles, system complexity and cost problem, several non-imaging techniques are proposed.

The 25∼34 GHz with ten frequency steps monostatic mmW imaging system using a CSOM that realizes adaptive clustering of complex-valued texture in space and frequency domain to reconstruct image is developed by Onojima *et al.* [10], [79]. CSOM pays more attention to phase information, which basically represents target distance, to suppress the harmful speckles. It consists of feature vector extraction and adaptive classification. The extracted feature vectors represent local complex-amplitude textural quantity in a local window all over the image. The amplitude information in 3D raw data is converted into decibel (dB) representation, while the phase information remains unchanged, so that the data stability could be higher. Then a local window block for each element in space and frequency domain is prepared respectively, and the local correlations in space domain K_s and those in frequency domain K_f in the block are calculated. The complex-valued mean M is also a part of feature vector, and the feature vectors K described as $[M, K_s, K_f]$ finally. The adaptive classification has two steps. Firstly, some reference vectors representing respective classes at random are prepared. Secondly, for the feature vectors K of each pixel, a winner reference vector that is located nearest to K with the complex-valued inner-product metric is determined. Finally, the winner reference vector and its neighbors are updated. The complex-valued inner-product pay more attention to the phase information, and is inherently less sensitive to the norm of signal vectors when the amplitude has larger variance. It is the desirable method for solving the image distortion problems caused by the mirror glaring and speckles in

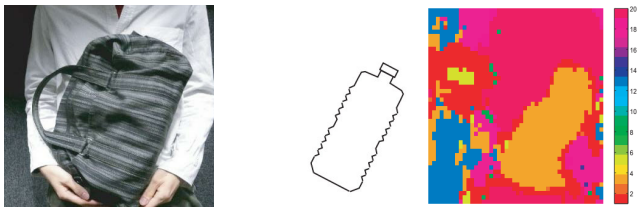

FIGURE 9. Measurement scenario (a) with a plastic (PET) bottle in a bag (b), and the reconstructed image with CSOM (c).

mmW imaging. The proposed CSOM active mmW imaging system is especially suitable for detecting object having mirror glaring and speckles, and a PET bottle filled with water in a bag on human body is detected successfully, as shown in Fig. 9.

The 60.025∼61.825 GHz mmW system using the frequency encoding technique is proposed by Derham *et al.* [80]. The system has a standard horn antenna as the transmitter, and a receiver antenna with 2D reflector. The image is reconstructed by frequency encoding and mechanical scanning. The scanning in azimuth and elevation is achieved by use of two motors. The frequency encoding over the 9.5° scanning range is used to form the image, resulting in the image with approximately 45° by 30° FOV. The experiments show that the proposed frequency encoding technique could effectively restrain the distortion caused by the specular reflections from the flat obstacle surface.

The 76.5 GHz modulated by a sinusoidal AM at a 0.05∼1 GHz low frequency monostatic mmW imaging system using the envelope phase detection method is proposed by Radenamad *et al.* [30], [81]. The transmitter emits mmW with AM, while the receiver detects the scattered signal directly with an envelope detector. The envelope phase of the AM is used to obtain the 3D image by the use of phase unwrapping. Since there is no need for synthetic aperture and digital focusing, the imaging time could be reduced. Additionally, the envelope phase detection method could suppress harmful speckles, and render the shape of the object to appear more clearly.

Similarly, the 94 GHz modulated by an AM at 1 kHz mmW imaging system is designed by Kapilevich and Einat [82]. The system also uses the diode detector to detect the power of the signal scattered by the target. Additionally, a time gating algorithm combined with pre-determined threshold level is implemented in the low-cost system, and experiments show that the detection probability of 90% or more for metal and plastic concealed objects at a distance up to 3 m is achieved.

For standoff range detection, there are also several systems implementing non-imaging techniques developed for personnel security screening. The linearly polarized 75∼110 GHz standoff mmW system with a Gaussian optic lens antenna is developed by Andrews *et al.* [18]. The receivers only measure the power of the signals scattered by the target. Although the information contained within the waveform is reduced, the range information of the target is still retrievable by performing an inverse FT. In the digital process, neural network processes the scattered polarimetric, range domain waveforms, and achieves threat detection autonomously. The system is portable and manually steered by the operator to enable up to 25 m standoff detecting of on-the-move human targets at 30 fps video frame rates.

The systems mentioned above all have an essential common characteristic. Instead of complete amplitude and phase information of the signals scattered by the targets, a certain feature value better representing the characteristics of the interested targets, such as the feature vector in CSOM, frequency encoding, and scattered signal power, is used to reconstruct the image and identify the target [80], [83]. Since only partial information contained within the scattered signal is processed and utilized, the systems have the advantages of fast detection and low cost.

IV. APPLICATION CONSIDERATIONS

A. SYSTEM CALIBRATION

The performance of an actual mmW imaging system is inevitably influenced by the errors within the mmW signal generation, distribution and processing. The errors generated during signal processing can be divided into random errors and systematic errors. The random errors are mainly caused by phase noise of the source and electromagnetic interferences (EMI) of the power supply, and lead to an increased noise level of the image. The systematic errors come from crosstalk between channels and signal delay [84]–[86].

Therefore, proper calibration is vital for optimizing the performance of mmW imaging systems. Intuitively, calibration for suppressing errors could be performed by referencing the scattered signal from a standard calibration target. In a monostatic mmW imaging system [69], a large piece of absorbing material covering the whole scanned aperture in front of the antenna array is used to obtain the errors S_e, while a large metal plate is used to get the plate response with errors S_o. Therefore, the calibrated signal can be expressed by

$$S_c = \frac{S_o - S_e}{S_s} S_i, \tag{17}$$

where S_o represents the measurement with errors, S_e the errors, S_s the real metal plate response with errors, S_i the ideal response of the ideal metal plate with infinite size and total reflection. And similar calibration is also used in the cylindrical and multistatic imaging systems [26], [84], [87].

B. WALK-THROUGH SYSTEMS (WTS)

The existing active mmW imaging systems for personnel security screening have been widely used over the world and proven to offer good results in the detection of metallic and non-metallic threats such as handguns, explosives, and ceramic knives. However, all of them have some limitations in field applications. During the screening process the passenger has to cooperate by adopting a specific position and posture for a certain length of time, or performing a specific movement in front of the system [46], [74], [88]. Therefore, the

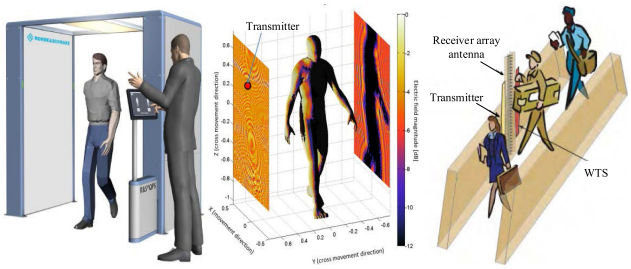

FIGURE 10. Sketches of WTS based on existing imaging systems.

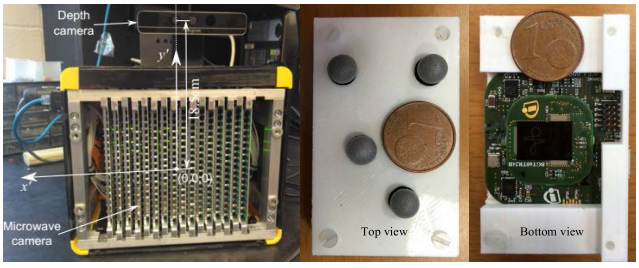

FIGURE 11. Portable systems using the optical depth camera (a) and the optical positioning system (b).

throughput is lower compared to the inspection with conventional security detection systems [31], [32], [89]. For another, the development of checkpoints that allow high throughput is becoming a priority, and the International Air Transport Association (IATA) declared that "from 2020 and beyond it is envisaged that the passenger will be able to flow through the security checkpoint without interruption."

To solve the problem, the concept of a mmW WTS is proposed. WTS would be more friendly to the passenger and would offer a higher throughput, which is a key parameter for field applications. Furthermore, a full illumination of the person is achieved by combining all recorded frames, and the detection of possible threats is improved [86]. The WTS prototype is commonly achieved by use of existing mmW imaging systems.

The concept of WTS based on the perimeter multistatic sparse array is demonstrated by Gumbmann and Ahmed, as shown in Fig. 10 (a) [31]. The proposed WTS consists of two synchronized imaging systems with 1.5 m distance. Each system works in the 70∼80 GHz frequency range, consists of 3008 transmit and receive antennas covering an area of 1 m by 2 m, and uses the MIMO RMA for image generation. When the passenger enters the WTS, the initial measurements offer the illumination of the front. When the passenger passes the WTS, both side measurements are obtained. And when the passenger leaves the passageway, the back of passenger is scanned.

Similarly, the WTS based on inhomogeneous multistatic sparse array, called on-the-moving imaging system, is introduced by Gonzalez-Valdes et al., as shown in Fig. 10 (b) [32], [89]. There are also two planes containing transceiver antennas placed on both sides of the passageway. The transmitters and receivers are separated with a subtended angle relative to the passenger equal to or greater than 90 ° to capture information from all possible mmW incident and scattering angles. For each transmitter, the scattered field is collected by all of the receivers on both sides. And for receiver array on each side, a recontructed image is achieved. When the passenger moves along the passageway, the imaging results could be obtained. The imaging method is usually based on MIMO RMA.

Based on the CSOM mmW imaging system, a WTS with a linear antenna array is proposed by Arima and Hirose, as shown in Fig. 10 (c) [10]. This WTS consists of a parallel front end including a linear array parallel antenna, and a CSOM to deal with complex texture. By use of the CSOM image processing, it is possible to realize a high throughput because it is unnecessary for the passenger to stop walking. Apparently, two synchronized CSOM WTS's placed on either side of the walkway could achieve full visualization for personnel security detection.

In essence, WTS is a novel system configuration method to trade space for time. The transceiver arrays are placed on both sides of the passageway, the scattered signals could be received continuously during the movement of the passenger when passing through the imaging system, and the total detection time is virtually added. The detection performance could be enhanced since possible concealed threats are visible from different perspectives and could be tracked within different frames.

C. PORTABLE SYSTEMS

To resolve the conflict between compactness requirements in applications and mannequin-size FOV as well as reasonable cross-range resolution, portable imaging systems combining mmW imaging and other auxiliary techniques, such as an optical camera and a positioning system, are proposed [33], [34]. A portable mmW imaging system based on the monostatic SAR and the optical depth camera was proposed by Laviada *et al.* [33], as shown in Fig. 11 (a). With the help of the camera, the entire system can be arbitrarily moved around the object being imaged, and reconstructs the image by use of classical RMA and position estimation derived from the camera. The mmW imaging system combined with an optical depth camera enables a coverage area much larger than that possible with a compact portable imaging system, and allows for incorporation of multi-views to improve the overall image quality. The portable system could provide a continuously-updated image with a refresh rate of approximately 1.5 seconds. Another compact mmW imaging system based on a 20∼30 GHz FMCW monostatic module and an optical positioning system was presented by Alvarez-Narciandi *et al.* [34], as shown in Fig. 11 (b). The position of the system is tracked by means of the positioning system for allowing the free movements of the system to create a synthetic aperture much larger than the system size. In contrast with the WTS, the portable mmW imaging systems

reduce the size at the cost of mannequin size scanning time. With the space information provided by auxiliary techniques, the compact aperture is equivalently synthesized to produce a large aperture, and the multiple frames are fused together for reconstructing the image.

D. COMPRESSIVE SENSING (CS)

Most commercial portal active mmW imaging systems are based on SAR with monostatic or multistatic arrays. Either a monostatic or a multistatic system has an effective 2D antenna aperture by mechanical or electrical scanning [90], [91]. From the mechanical point of view, fast scanning depends on the function of high performance servo motor and high accuracy mechanical structure. Existing related devices are difficult to meet the mmW real-time imaging requirements. Electronic scanning provides a faster and more reliable solution, but at the expense of increasing the number of antennas and the additional cost of the imaging system [92]. Multistatic systems with sparse arrays have the advantage of reducing the antennas number. However, the reduced number is in comparison with dense array. Theoretically, the formed 2D antenna array must satisfy the Nyquist sampling theorem, and the effective antenna element spacing is traditionally half wavelength. Therefore, sparseness in multistatic array has limitations.

Fortunately, a novel signal processing technique known as compressive sensing (CS) was propose by Candes and Wakin [93], [94], which can potentially solve this dilemma. According to the CS theory, a signal can be recovered from far fewer measurements than that dictated by the Nyquist criterion by exploiting the known signal sparsity. That is, the feasibility of reconstructing mmW images from scattered signals could be obtained with antenna array having double, triple or even larger Nyquist spacing, so long as the elements used for the reconstruction of image have sparsity and the sampling is random or incoherent with respect to the measured signal. The number of antennas, as well as system cost and complexity, could be reduced dramatically.

Initially, CS approach is tentatively used in an mmW imaging system by Cull *et al.* [95]. The 3D reconstructed images from the common amplitude and phase information and from the randomly subsampled measurements are compared. To analyze the impact of subsampled measurements on reconstructed image, a binary valued, pseudorandom transmittance function for reducing the number of measurements is applied, and the total variation (TV) sparsity base is adapted for the measurement subsampling. Simulations and experimental reconstructed images show that randomly sampled measurements, even with the 54.68% of the measurements removed, still achieve the reconstructed image. Furthermore, three sparsity bases, including TV, wavelet, and curvelet, are evaluated for the CS reconstruction performance in the monostatic mmW imaging system [35]. The feasibility of reconstructed images from measurements at half or even a quarter of the Nyquist samples is demonstrated. CS is also used in mmW imaging systems with bistatic array where one fixed transmitter antenna and a linear array of receiving antennas [36], cylindrical configuration [37] and planar phased array [38], [39]. The main advantages of these methods include the reduction of the scanning time and quality improvement of the reconstructed image. However, compared to the classical RMA digital focusing method, CS increases the digital processing time, making it a challenge to use CS in most commercial mmW imaging systems [96]–[98].

V. CONCLUSION

This paper reviews the research history of active mmW imaging systems for personnel security screening, and the associated imaging techniques, highlighting research activities and achievements, along with antenna considerations based on quasi-optical geometry, phased reflector array, monostatic array, and multistatic array. Detailed imaging techniques using quasi-optical focusing, digital focusing and non-imaging method are summarized. Design considerations and improvements related to practical applications, including system calibration, walk-through system (WTS), portable system, and compressive sensing (CS), are also discussed. In these aspects the review strives to be comprehensive. Nonetheless, important facets such as post processing techniques are equally interesting and relevant, but due to limitations of space, have to be relegated to a future review.

APPENDIX

Maxwell's equations in the frequency-domain representation in a source-free region for an isotropic linear inhomogeneous material with permittivity $\varepsilon(r)$ and permeability $\mu(r)$ are

$$\nabla \times E = -j\omega\mu(r)H, \tag{A1-1}$$

$$\nabla \times H = j\omega\varepsilon(r)E, \tag{A1-2}$$

$$\nabla \cdot (\varepsilon(r)E) = 0, \tag{A1-3}$$

$$\nabla \cdot (\mu(r)H) = 0, \tag{A1-4}$$

where E and H denote the 3D vector quantities of the electric field and the magnetic field respectively, ω the electromagnetic wave angular frequency, r a 3D position vector in the space.

By dividing (A1-1) with $\mu(r)$, and applying a curl operation to both sides, (A1-1) becomes

$$\nabla \times \left(\frac{\nabla \times E}{\mu(r)}\right) = -j\omega\nabla \times H. \tag{A2}$$

There are several general vector identities for a scalar field and a vector field that can be used to manipulate the vector-differential operations in the above equation, such as

$$\nabla \times (\alpha\Psi) = \alpha(\nabla \times \Psi) + (\nabla\alpha) \times \Psi, \tag{A3-1}$$

$$\nabla \times \nabla \times \Psi = \nabla(\nabla \cdot \Psi) - \nabla^2\Psi, \tag{A3-2}$$

$$\nabla \cdot (\alpha\Psi) = (\nabla\alpha) \cdot \Psi + \alpha(\nabla \cdot \Psi), \tag{A3-3}$$

$$\frac{\nabla\alpha}{\alpha} = -\nabla(\ln(\alpha)), \tag{A3-4}$$

$$\alpha\nabla\left(\frac{1}{\alpha}\right) = \nabla(\ln(\alpha)), \tag{A3-5}$$

where α and Ψ represent a scalar field and a vector field respectively.

By substituting (A1-2) into (A2), and applying identity (A3-1), (A2) becomes

$$\nabla^2 E + \omega^2 \mu(r)\,\varepsilon(r)\,E = (\nabla \ln \mu(r)) \times (\nabla \times E) - \nabla((\nabla \ln \varepsilon(r)) \cdot E). \quad \text{(A4)}$$

REFERENCES

[1] D. M. Sheen, J. L. Fernandes, J. R. Tedeschi, D. L. McMakin, and A. M. Jones, W. M. Lechelt, and R. H. Severtsen, "Wide-bandwidth, wide-beamwidth, high-resolution, millimeter-wave imaging for concealed weapon detection," *Proc. SPIE*, vol. 8715, p. 871509, May 2013.

[2] S. S. Ahmed, "Advanced fully-electronic personnel security screening technology," in *Proc. 9th EuCAP*, Lisbon, Portugal, Apr. 2015, pp. 1–4.

[3] J. E. Bjarnason, T. L. J. Chan, A. W. M. Lee, M. A. Celis, and E. R. Brown, "Millimeter-wave, terahertz, and mid-infrared transmission through common clothing," *Appl. Phys. Lett.*, vol. 85, no. 4, pp. 519–521, Apr. 2004.

[4] D. M. Sheen, D. L. McMakin, T. E. Hall, and R. H. Severtsen, "Active millimeter-wave standoff and portal imaging techniques for personnel screening," in *Proc. IEEE Conf. Technol. Homeland Secur.*, Boston, MA, USA, May 2009, pp. 440–447.

[5] D. M. Sheen, D. L. McMakin, and T. E. Hall, "Three-dimensional millimeter wave imaging for concealed weapon detection," *IEEE Trans. Microw. Theory Techn.*, vol. 49, no. 9, pp. 1581–1592, Sep. 2001.

[6] Y. Zhu, M. Yang, L. Wu, Y. Sun, and X. Sun, "Millimeter-wave holographic imaging algorithm with amplitude corrections," *Prog. Electromagn. Res. M*, vol. 49, no. 9, pp. 33–39, Jul. 2016.

[7] D. M. Sheen and T. E. Hall, "Calibration, reconstruction, and rendering of cylindrical millimeter wave image data," *Proc. SPIE*, vol. 8022, p. 80220H, May 2011.

[8] L3 Harris Security & Detection Systems. (2019). *ProVision 2 Compact, Image-Free People Security scanner*. Accessed: Jul. 25, 2019. [Online]. Available: https://www.sds.l3t.com/advancedimaging/provision-2.htm

[9] Xinhua. (2018). *Millimeter Wave Tech Introduced Into Airports Checks*. Accessed: Jul. 2, 2018. [Online]. Available: http://www.china.org.cn/china/2018-07/02/content_54445754.htm

[10] S. Onojima, Y. N. Arima, and A. Hirose, "Millimeter-wave security imaging using complex-valued self-organizing map for visualization of moving targets," *Neurocomputing*, vol. 134, no. 25, pp. 247–253, Jun. 2014.

[11] P. F. Goldsmith, C.-T. Hsieh, G. R. Huguenin, J. Kapitzky, and E. L. Moore, "Focal plane imaging systems for millimeter wavelengths," *IEEE Trans. Microw. Theory Techn.*, vol. 41, no. 10, pp. 1664–1675, Oct. 1993.

[12] N. H. Farhat and W. R. Guard, "Millimeter wave holographic imaging of concealed weapons," *Proc. IEEE*, vol. 59, no. 9, pp. 1383–1384, Sep. 1971.

[13] K. B. Cooper, R. J. Dengler, N. Llombart, T. Bryllert, G. Chattopadhyay, G. Chattopadhyay, J. Gill, C. Lee, A. Skalare, I. Mehdi, and P. H. Siegel, "Penetrating 3-D imaging at 4- and 25-m range using a submillimeter-wave radar," *IEEE Trans. Microw. Theory Techn.*, vol. 56, no. 12, pp. 2771–2778, Dec. 2008.

[14] K. B. Cooper, R. J. Dengler, G. Chattopadhyay, E. Schlecht, J. Gill, A. Skalare, I. Mehdi, and P. H. Siegel, "A high-resolution imaging radar at 580 GHz," *IEEE Microw. Wireless Compon. Lett.*, vol. 18, no. 1, pp. 64–66, Jan. 2008.

[15] D. M. Sheen, T. E. Hall, R. H. Severtsen, D. L. McMakin, B. K. Hatchell, and P. L. J. Valdez, "Active wideband 350 GHz imaging system for concealed-weapon detection," *Proc. SPIE*, vol. 7309, p. 730901, Apr. 2009.

[16] D. A. Robertson, P. N. Marsh, D. R. Bolton, R. J. C. Middleton, R. I. Hunter, P. J. Speirs, D. G. Macfarlane, S. L. Cassidy, and G. M. Smith, "340 GHz 3D radar imaging test bed with 10 Hz frame rate," *Proc. SPIE*, vol. 8362, p. 836206, May 2012.

[17] P. F. Goldsmith, "Perforated plate lens for millimeter quasi-optical systems," *IEEE Trans. Antennas Propag.*, vol. 39, no. 6, pp. 834–838, Jun. 1991.

[18] D. A. Andrews, S. W. Harmer, N. J. Bowring, N. D. Rezgui, and M. J. Southgate, "Active millimeter wave sensor for standoff concealed threat detection," *IEEE Sensors J.*, vol. 13, no. 12, pp. 4948–4954, Dec. 2013.

[19] K. J. Roe and C. W. Gregory, "Wave-based sensing and imaging for security applications," in *Proc. 9th EuCAP*, Lisbon, Portugal, Apr. 2015, pp. 1–5.

[20] H. D. Collins, D. L. McMakin, T. E. Hall, and R. P. Gribble, "Real-time holographic surveillance system," U.S. Patent 5 455 590, Oct. 3, 1995.

[21] D. M. Sheen, H. D. Collins, T. E. Hall, D. L. McMakin, R. P. Cribble, R. H. Severtsen, J. M. Prince, and L. D. Reid, "Real-time holographic surveillance system," U.S. Patent 5 557 283, Sep. 17, 1996.

[22] D. M. Sheen, D. L. McMakin, H. D. Collins, T. E. Hall, and R. H. Severtsen, "Concealed explosive detection on personnel using a wideband holographic millimeter wave imaging system," *Proc. SPIE*, vol. 2755, pp. 503–513, Jun. 1996.

[23] D. L. McMakin, D. M. Sheen, J. W. Griffin, and W. M. Lechelt, "Extremely high-frequency holographic radar imaging of personnel and mail," *Proc. SPIE*, vol. 6201, p. 62011W, May 2006.

[24] D. M. Sheen, D. L. McMakin, W. M. Lechelt, and J. W. Griffin, "Circularly polarized millimeter-wave imaging for personnel screening," *Proc. SPIE*, vol. 5789, p. 117, May 2005.

[25] D. M. Sheen, D. L. McMakin, T. E. Hall, and R. H. Severtsen, "Real-time wideband cylindrical holographic surveillance system," U.S. Patent 5 859 609, Nov. 23, 2004.

[26] D. M. Sheen, D. L. McMakin, and T. E. Hall, "Cylindrical millimeter-wave imaging technique and applications," *Proc. SPIE*, vol. 6211, p. 62110A, May 2006.

[27] D. M. Sheen, D. L. McMakin, and T. E. Hall, "Near field imaging at microwave and millimeter wave frequencies," in *IEEE MTT-S Int. Microw. Symp. Dig.*, Honolulu, HI, USA, Jun. 2007, pp. 1693–1696.

[28] J. L. Fernandes, C. M. Rappaport, and D. M. Sheen, "Improved reconstruction and sensing techniques for personnel security screening in three-dimensional cylindrical millimeter-wave portal scanning," *Proc. SPIE*, vol. 8022, p. 802205, May 2011.

[29] S. S. Ahmed, A. Schiessl, and L.-P. Schmidt, "A novel fully electronic active real-time imager based on a planar multistatic sparse array," *IEEE Trans. Microw. Theory Techn.*, vol. 59, no. 12, pp. 3567–3576, Dec. 2011.

[30] D. Radenamad, T. Aoyagi, and A. Hirose, "High-sensitivity millimeter-wave imaging front-end using a low-impedance tapered slot antenna," *IEEE Trans. Antennas Propag.*, vol. 59, no. 12, pp. 4868–4872, Dec. 2011.

[31] F. Gumbmann and S. S. Ahmed, "Walk through screening with multistatic mmW technology," *Proc. SPIE*, vol. 9993, p. 999306, Oct. 2016.

[32] B. Gonzalez-Valdes, Y. Álvarez, Y. Rodriguez-Vaqueiro, A. Arboleya-Arboleya, A. García-Pino, C. M. Rappaport, F. Las-Heras, and J. A. Martinez-Lorenzo, "Millimeter wave imaging architecture for on-the-move whole body imaging," *IEEE Trans. Antennas Propag.*, vol. 64, no. 6, pp. 2328–2338, Jun. 2016.

[33] J. Laviada, M. T. Ghasr, M. Lopez-Portugues, F. Las-Heras, and R. Zoughi, "Real-time multi-view SAR imaging using a portable microwave camera with arbitrary movement," *IEEE Trans. Antennas Propag.*, vol. 66, no. 12, pp. 7305–7314, Dec. 2018.

[34] G. Alvarez-Narciandi, M. Lopez-Portugues, F. Las-Heras, and J. Laviada, "Freehand, agile, and high-resolution imaging with compact mm-wave radar," *IEEE Access*, vol. 7, pp. 95516–95526, Jul. 2019.

[35] L. Qiao, Y. Wang, Z. Zhao, and Z. Chen, "Total variance regularization for millimeter-wave holographic imaging," in *Proc. 39th IRMMW-THz*, Tucson, AZ, USA, Sep. 2014, pp. 1–2.

[36] A. Farsaei1, F. Mokhtari-Koushyar, S. Seyed-Talebi, Z. Kavehvash, and M. Shabany, "Improved two-dimensional millimeter-wave imaging for concealed weapon detection through partial Fourier sampling," *J. Infr. Milli. THz Waves*, vol. 37, no. 3, pp. 267–280, Mar. 2016.

[37] G. Zhao, S. Li, B. Ren, Q. Qiu, and H. Sun, "Cylindrical three-dimensional millimeter-wave imaging via compressive sensing," *Int. J. Antenn. Propag.*, vol. 2015, p. 218751, Jul. 2015.

[38] Q. Cheng, A. Alomaing, and Y. Hao, "On the performance of compressed sensingbased methods for millimeter-wave holographic imaging," *Appl. Opt.*, vol. 55, no. 4, pp. 728–738, Feb. 2016.

[39] Q. Cheng, A. Alomainy, and Y. Hao, "Compressive millimeter-wave phased array imaging," *IEEE Access*, vol. 4, pp. 9580–9588, 2016.

[40] S. S. Ahmed, "Multistatic array imaging," in *Electronic Microwave Imaging With Planar Multistatic Arrays*. Erlangen, Germany: Friedrich-Alexander-Universität Erlangen-Nürnberg, 2013.

[41] E. Wolf, "Three-dimensional structure determination of semitransparent objects from holographic data," *Opt. Commun.*, vol. 1, no. 4, pp. 153–156, 1969.

[42] R. Appleby and H. B. Wallace, "Standoff detection of weapons and contraband in the 100 GHz to 1 THz region," *IEEE Trans. Antennas Propag.*, vol. 55, no. 11, pp. 2944–2956, Nov. 2007.

[43] G. Tricoles and N. H. Farhat, "Microwave holography: Applications and techniques," *Proc. IEEE*, vol. 65, no. 1, pp. 108–121, Jan. 1977.

[44] M. Younis, C. Fischer, and W. Wiesbeck, "Digital beamforming in SAR systems," *IEEE Trans. Geosci. Remote Sens.*, vol. 41, no. 7, pp. 1735–1739, Jul. 2003.

[45] R. Zhu, J. Zhou, G. Jiang, and Q. Fu, "Range migration algorithm for near-field MIMO-SAR imaging," *IEEE Geosci. Remote Sens. Lett.*, vol. 14, no. 12, pp. 2280–2284, Dec. 2017.

[46] C. A. Weg, W. V. Spiegel, R. Henneberger, R. Zimmermann, T. Loeffler, and H. G. Roskos, "Fast active THz cameras with ranging capabilities," *J. Infr. Millim. THz Waves*, vol. 30, no. 12, pp. 1281–1296, Dec. 2009.

[47] N. Llombart, K. B. Cooper, R. J. Dengler, T. Bryllert, and P. H. Siegel, "Confocal ellipsoidal reflector system for a mechanically scanned active terahertz imager," *IEEE Trans. Antennas Propag.*, vol. 58, no. 6, pp. 1834–1841, Jun. 2010.

[48] K. B. Cooper and G. Chattopadhyay, "Submillimeter-wave radar: Solid-state system design and applications," *IEEE Microw. Mag.*, vol. 15, no. 7, pp. 51–67, Nov. 2014.

[49] K. B. Cooper, R. J. Dengler, N. Llombart, B. Thomas, G. Chattopadhyay, and P. H. Siegel, "THz imaging radar for standoff personnel screening," *IEEE Trans. THz Sci. Technol.*, vol. 1, no. 1, pp. 169–182, Jun. 2011.

[50] K. B. Cooper, R. J. Dengler, N. Llombart, A. Talukder, A. V. Panangadan, C. S. Peay, I. Mehdi, and P. H. Siegel, "Fast high-resolution terahertz radar imaging at 25 meters," *Proc. SPIE*, vol. 7671, p. 76710Y, Apr. 2010.

[51] G. Chattopadhyay, K. B. Cooper, R. Dengler, T. E. Bryllert, E. Schlecht, A. Skalare, I. Mehdi, and P. H. Siegel, "A 600 GHz imaging radar for contraband detection," in *Proc. 19th Int. Symp. Space THz Tech.*, Groningen, The Netherlands, Apr. 2008, pp. 28–30.

[52] A. Garcia-Pino, N. Llombart, B. Gonzalez-Valdes, and O. Rubinos-Lopez, "A bifocal ellipsoidal Gregorian reflector system for THz imaging applications," *IEEE Trans. Antennas Propag.*, vol. 60, no. 9, pp. 4119–4129, Sep. 2012.

[53] J. Grajal, A. Badolato, G. Rubio-Cidre, L. Úbeda-Medina, B. Mencia-Oliva, A. Garcia-Pino, B. Gonzalez-Valdes, and O. Rubiños, "3-D high-resolution imaging radar at 300 GHz with enhanced FoV," *IEEE Trans. Microw. Theory Techn.*, vol. 63, no. 3, pp. 1097–1107, Mar. 2015.

[54] A. Garcia-Pino, B. Gonzalez-Valdes, O. Rubiños, J. Grajal, A. Badolato, B. Mencia-Oliva, P. G. Soidán, and J. L. Besada-Sanmartín, "Bifocal reflector antenna for a standoff radar imaging system with enhanced field of view," *IEEE Trans. Antennas Propag.*, vol. 62, no. 10, pp. 4997–5006, Oct. 2014.

[55] P. Corredoura, Z. Baharav, B. Taber, and G. Lee, "Millimeter-wave imaging system for personnel security screening: Scanning 107 points a second and using no moving parts," *Proc. SPIE*, vol. 6211, p. 62110B, May 2006.

[56] B. N. Lyons, E. Entchev, and M. K. Crowley, "Reflect-array based mm-wave people screening system," *Proc. SPIE*, vol. 8900, p. 890002, Oct. 2013.

[57] D. M. Pozar, S. D. Targonski, and H. D. Syrigos, "Design of millimeter wave microstrip reflectarrays," *IEEE Trans. Antennas Propag.*, vol. 45, no. 2, pp. 287–296, Feb. 1997.

[58] Y. Zhang, B. Deng, Q. Yang, J. Gao, Y. Qin, and H. Wang, "Near-field three-dimensional planar millimeter-wave holographic imaging by using frequency scaling algorithm," *Sensors*, vol. 17, no. 10, pp. 2438–2451, 2017.

[59] T. Reck, C. Jung-Kubiak, J. V. Siles, C. Lee, R. Lin, and G. Chattopadhyay, "A silicon micromachined eight-pixel transceiver array for submillimeter-wave radar," *IEEE Trans. THz Sci. Technol.*, vol. 5, no. 2, pp. 197–206, Mar. 2015.

[60] M. T. Ghasr, M. J. Horst, M. R. Dvorsky, and R. Zoughi, "Wideband microwave camera for real-time 3D imaging," *IEEE Trans. Antennas Propag.*, vol. 65, no. 1, pp. 258–268, Jan. 2017.

[61] A. Redo-Sanchez, G. Kaur, X. C. Zhang, F. Buersgens, and R. Kersting, "2-D acoustic phase imaging with millimeter-wave radiation," *IEEE Trans. Microw. Theory Techn.*, vol. 57, no. 3, pp. 589–593, Mar. 2009.

[62] M. Fallahpour, J. T. Case, M. T. Ghasr, and R. Zoughi, "Piecewise and Wiener filter-based SAR techniques for monostatic microwave imaging of layered structures," *IEEE Trans. Antennas Propag.*, vol. 62, no. 1, pp. 282–294, Jan. 2014.

[63] D. Gabor, "A new microscopic principle," *Nature*, vol. 161, no. 4098, pp. 777–778, May 1948.

[64] M. Soumekh, "Bistatic synthetic aperture radar inversion with application in dynamic object imaging," *IEEE Trans. Signal Process.*, vol. 39, no. 9, pp. 2044–2055, Sep. 1991.

[65] M. Soumekh, "A system model and inversion for synthetic aperture radar imaging," *IEEE Trans. Image Process.*, vol. 1, no. 1, pp. 64–76, Jan. 1992.

[66] Y. Sasaki, F. Shang, S. Kidera, T. Kirimoto, K. Saho, and T. Sato, "Three-dimensional imaging method incorporating range points migration and Doppler velocity estimation for UWB millimeter-wave radar," *IEEE Geosci. Remote Sens. Lett.*, vol. 14, no. 1, pp. 122–126, Jan. 2017.

[67] A. Dutt and V. Rokhlin, "Fast Fourier transforms for nonequispaced data," *SIAM J. Sci. Comput.*, vol. 14, no. 6, pp. 1368–1393, 1993.

[68] J. Camacho, M. Parrilla, and C. Fritsch, "Phase coherence imaging," *IEEE Trans. Ultrason., Ferroelectr., Freq. Control*, vol. 56, no. 5, pp. 958–974, May 2009.

[69] L. Qiao, Y. Wang, Z. Zhao, and Z. Chen, "Exact reconstruction for near-field three-dimensional planar millimeter-wave holographic imaging," *J. Infr. Millim. THz Waves*, vol. 36, no. 12, pp. 1221–1236, Oct. 2015.

[70] Q. Guo, J. Wang, T. Chang, and H. L. Cui, "Dimension-factorized range migration algorithm for regularly distributed array imaging," *Sensors*, vol. 17, no. 11, pp. 2549–2552, Nov. 2017.

[71] Q. Guo, T. Chang, G. Geng, C. Jia, and H. L. Cui, "A high precision terahertz wave image reconstruction algorithm," *Sensors*, vol. 16, no. 7, pp. 1139–1154, Jul. 2016.

[72] R. Zhang and S. Cao, "3D imaging millimeter wave circular synthetic aperture radar," *Sensors*, vol. 17, no. 16, pp. 1419–1439, Jun. 2017.

[73] X. Zhuge and A. G. Yarovoy, "Three-dimensional near-field MIMO array imaging using range migration techniques," *IEEE Trans. Image Process.*, vol. 21, no. 6, pp. 3026–3033, Jun. 2012.

[74] W. F. Moulder, J. D. Krieger, J. J. Majewski, C. M. Coldwell, H. T. Nguyen, D. T. Maurais-Galejs, T. L. Anderson, P. Dufilie, and J. S. Herd, "Development of a high-throughput microwave imaging system for concealed weapons detection," in *Proc. IEEE Int. Symp. Phased Array Syst. Techn.*, Waltham, MA, USA, Oct. 2017, pp. 1–6.

[75] Z. Wang, Q. Guo, X. Tian, T. Chang, and H.-L. Cui, "Near-field 3-D millimeter-wave imaging using MIMO RMA with range compensation," *IEEE Trans. Microw. Theory Techn.*, vol. 67, no. 3, pp. 1157–1166, Mar. 2019.

[76] J. N. Gollub, O. Yurduseven, K. P. Trofatter, D. Arnitz, M. F. Imani, T. Sleasman, M. Boyarsky, A. Rose, A. Pedross-Engel, H. Odabasi, T. Zvolensky, G. Lipworth, D. Brady, D. L. Marks, M. S. Reynolds, and D. R. Smith, "Large metasurface aperture for millimeter wave computational imaging at the human-scale," *Sci. Rep.*, vol. 7, no. 42650, pp. 1–8, Feb. 2017.

[77] S. W. Harmer, N. Bowring, D. Andrews, N. D. Rezgui, M. Southgate, and S. Smith, "A review of nonimaging stand-off concealed threat detection with millimeter-wave radar," *IEEE Microw.*, vol. 13, no. 1, pp. 160–167, Jan. 2012.

[78] G. Brooker and D. G. Johnson, "Low-cost millimeter wave imaging using a commercial plasma display," *IEEE Sensors J.*, vol. 15, no. 6, pp. 3557–3564, Jun. 2015.

[79] Y. Arima and A. Hirose, "Performance dependence on system parameters in millimeter-wave active imaging based on complex-valued neural networks to classify complex texture," *IEEE Access*, vol. 5, pp. 22927–22939, Sep. 2017.

[80] T. Derham, H. Kamoda, T. Iwasaki, and T. Kuki, "Active MMW imaging system using the frequency-encoding technique," in *Proc. Korea-Japan Microw. Conf.*, Okinawa, Japan, Nov. 2007, pp. 181–184.

[81] A. Hirose, S. Hamada, and R. Yamaki, "Envelope phase detection for millimetre-wave active imaging," *Electron. Lett.*, vol. 45, no. 6, pp. 331–332, Mar. 2009.

[82] B. Kapilevich and M. Einat, "Detecting hidden objects on human body using active millimeter wave sensor," *IEEE Sensors J.*, vol. 10, no. 11, pp. 1746–1752, Nov. 2010.

[83] J. C. Weatherall, J. Barber, and B. T. Smith, "Spectral signatures for identifying explosives with wideband millimeter-wave illumination," *IEEE Trans. Microw. Theory Techn.*, vol. 64, no. 3, pp. 999–1005, Mar. 2016.

[84] A. Schiessl, A. Genghammer, S. S. Ahmed, and L. Schmidt, "Phase error sensitivity in multistatic microwave imaging systems," in *Proc. 43rd Eur. Microw. Conf.*, Nuremberg, Germany, Oct. 2013, pp. 1631–1634.

[85] A. Schiessl, S. S. Ahmed, A. Genghammer, and L. P. Schmidt, "Temperature sensitivity of large digital-beamforming multistatic mm-wave imaging systems," in *IEEE MTT-S Int. Microw. Symp. Dig.*, Seattle, WA, USA, 2013, pp. 1–3.

[86] A. Schiessl, S. S. Ahmed, and L.-P. Schmidt, "Motion effects in multistatic millimeter-wave imaging systems," *Proc. SPIE*, vol. 8900, p. 890007, Oct. 2013.
[87] A. Sharma, A. Pedross-Engel, D. Arnitz, C. M. Watts, D. R. Smith, and M. S. Reynolds, "A K-band backscatter fiducial for continuous calibration in coherent millimeter-wave imaging," *IEEE Trans. Microw. Theory Techn.*, vol. 66, no. 1, pp. 431–438, Jan. 2018.
[88] A. Arbabian, S. Callender, S. Kang, M. Rangwala, and A. M. Niknejad, "A 94 GHz mm-wave-to-baseband pulsed-radar transceiver with applications in imaging and gesture recognition," *IEEE J. Solid-State Circuits*, vol. 48, no. 4, pp. 1055–1071, Apr. 2013.
[89] B. Gonzalez-Valdes, Y. Alvarez, J. Gutiérrez-Meana, C. Rappaport, F. L. Heras, A. G. Pino, and J. A. Martinez-Lorenzo, "On-the-move millimeter wave imaging system using multiple transmitters and receivers," in *Proc. 9th EuCAP*, Lisbon, Portugal, Apr. 2015, pp. 1–4.
[90] S. Nowok, S. Kueppers, H. Cetinkaya, M. Schroeder, and R. Herschel, "Millimeter wave radar for high resolution 3D near field imaging for robotics and security scans," in *Proc. 18th Int. Radar Symp. IRS*, Prague, Czech Republic, Jun. 2017, pp. 1–10.
[91] J. Laviada, A. Arboleya-Arboleya, and F. Las-Heras, "Multistatic millimeter-wave imaging by multiview portable camera," *IEEE Access*, vol. 5, pp. 19259–19268, 2017.
[92] H. Zamani and M. Fakharzadeh, "1.5-D sparse array for millimeter-wave imaging based on compressive sensing techniques," *IEEE Trans. Antennas Propag.*, vol. 66, no. 4, pp. 2008–2015, Apr. 2018.
[93] E. J. Candès and M. B. Wakin, "An introduction to compressive sampling," *IEEE Signal Process. Mag.*, vol. 25, no. 2, pp. 21–30, Mar. 2008.
[94] D. L. Donoho, "Compressed sensing," *IEEE Trans. Inf. Theory*, vol. 52, no. 4, pp. 1289–1306, Apr. 2006.
[95] C. Cull, D. Wikner, J. Mait, M. Mattheiss, and D. Brady, "Millimeter-wave compressive holography," *Appl. Opt.*, vol. 49, no. 19, pp. 67–82, Jul. 2010.
[96] Y. Alvarez, Y. Rodriguez-Vaqueiro, B. Gonzalez-Valdes, C. Rappaport, F. Las-Heras, and J. Martinez-Lorenzo, "Three-dimensional compressed sensing-based millimeter-wave imaging," *IEEE Trans. Antennas Propag.*, vol. 63, no. 12, pp. 5868–5873, Dec. 2015.
[97] B. Gonzalez-Valdes, Y. Alvarez, S. Mantzavinos, C. M. Rappaport, F. Las-Heras, and J. Á. Martínez-Lorenzo, "Improving security screening: A comparison of multistatic radar configurations for human body imaging," *IEEE Antennas Propag. Mag.*, vol. 58, no. 4, pp. 35–47, Aug. 2016.
[98] J. Laviada, A. Arboleya-Arboleya, Y. Alvarez, B. Gonzalez-Valdes, and F. Las-Heras, "Multiview three-dimensional reconstruction by millimeter-wave portable camera," *Sci. Rep.*, vol. 7, no. 1, pp. 6479–6489, Jul. 2017.

ZHONGMIN WANG received the B.S. degree in automation from the School of Electrical Engineering, University of Jinan, Jinan, China, in 2005, and the M.S. degree in control theory and control engineering from the College of Control Science and Engineering, Shandong University, Jinan, in 2008. He is currently pursuing the Ph.D. degree with the College of Instrumentation and Electrical Engineering, Jilin University, Changchun, China. From 2009 to 2016, he was an Assistant Researcher with the Shandong Academy of Sciences, China. His research interests include millimeter wave imaging and optical fiber sensors.

TIANYING CHANG received the Ph.D. degree from the College of Control Science and Engineering, Shandong University, Jinan, China, in 2009. From 2007 to 2008, she was a joint Ph.D. Student with the Stevens Institute of Technology. She was a Lecturer with Shandong University, and a Postdoctoral Research Associate with New York University. She is currently an Associate Professor with Jilin University. Her research interests include optical fiber sensors, THz systems, and nano-optics.

HONG-LIANG CUI received the Ph.D. degree in theoretical physics from the Stevens Institute of Technology, in 1987, where he was a Professor of physics and engineering physics, and a Professor of applied physics with New York University. He is currently a Professor of electrical engineering with Jilin University. His research interests include solid-state electronics, fiber optic sensing, high-frequency electromagnetic wave propagation and interaction with matter, and physics-based approaches to modeling of semiconductor, and molecular devices.